Available online at www.sciencedirect.com

ScienceDirect

IFAC PapersOnline CONFERENCE PAPER ARCHIVE

IFAC PapersOnLine 51-15 (2018) 60–65

Nonlinear observer with observability-based parameter adaptation for vehicle motion estimation

Vicent Rodrigo Marco [*,**] **Jens Kalkkuhl** [**] **Thomas Seel** [*]

[*] *Control Systems Group, Department of Electrical Engineering and Computer Science, Technische Universität Berlin, D-10587 Berlin, Germany (e-mail: vicent.rodrigo_marco@daimler.com, seel@control.TU-berlin.de)*

[**] *Research and Development, Daimler AG, 71059 Sindelfingen, Germany (e-mail: jens.kalkkuhl@daimler.com)*

Abstract: In the framework of self-driving cars and driver-assistance systems the demand for reliable information about the vehicle ego-motion is increasing. This paper describes an estimation scheme, based on a nonlinear observer design, that provides velocity and attitude angle estimates. The approach relies on a state-affine representation of a kinematic model bolstered by a dynamic model-based measurement equation. By means of a thorough observability analysis, global exponential convergence is theoretically guaranteed. Additionally, in order to minimize the errors introduced by the dynamic model limitations, an observer tuning rule is proposed. The adaptation of the tuning parameters is built upon an online observability assessment of the system without the support of the dynamic model. Experimental results show that the presented approach reliably estimates the motion states.

Keywords: Motion estimation, observability, automobile industry, nonlinear systems.

1. INTRODUCTION

Accurate knowledge of the vehicle ego-motion is essential for autonomous driving and driver-assistance systems. The proper functioning of these systems relies on accurate information of the motion states, such as velocity and attitude angles. However, the direct measurement of all required states demands the usage of sophisticated sensors, which are too costly to be integrated in production cars. Hence, they must be estimated with the available information.

The estimation of the motion states has drawn scientific attention ever since the introduction of vehicle control systems. The proposed methods can be classified into dynamic and kinematic model-based approaches or a combination of both (Katriniok and Abel, 2016). Dynamic model-based methods rely on vehicle and tire models, which consider forces. Even though these methods are relatively robust against sensor errors, their accuracy is highly dependent on uncertainties in the vehicle and tire parameters (Hrgetic et al., 2014). Conversely, kinematic model-based methods are built upon kinematic differential equations describing the vehicle motion. Their advantage is the higher independence from uncertainties in the vehicle parameters. Nevertheless, since they are based on the angular rates and accelerations supplied by an inertial measurement unit (IMU), they are highly affected by sensor errors such as biases and scaling factors (Klier et al., 2008). In view of the lowering costs and performance improvements of Micro Electro Mechanical System (MEMS)-based inertial sensors, moving towards kinematic model-based methods appears reasonable. Combinations of the two approaches have also been suggested (Piyabongkarn et al., 2009). Recent publications have proposed the use of Global Navigation Satellite Systems (GNSS) and visual odometry to bolster the vehicle motion estimation (Katriniok and Abel, 2016; Weydert, 2012). However, in GNSS/camera-impaired environments, common in urban scenarios, the estimation accuracy is significantly affected.

In the area of vehicle motion estimation, stochastic estimators for nonlinear systems such as extended Kalman Filter (EKF), unscented Kalman Filter (UKF) and their multiple variants remain the prevailing used method in industry, e.g. Antonov et al. (2011); Brunker et al. (2017). In spite of providing fairly good performance in many engineering applications and having good local properties (Song and Grizzle, 1992), global convergence is generally not guaranteed. Conversely, deterministic observers, such as the so-called nonlinear observers (NLOs), are based on the Lyapunov stability theory and are theoretically globally converging (Bryne et al., 2017). Moreover, they are, in general, more computationally efficient. On the other hand, their performance may suffer in presence of noise and sampling. Furthermore, a systematic approach for all nonlinear systems remains a long-standing research question, and thus many of the available solutions aim at particular classes. In this context, Grip et al. (2009) developed a deterministic observer for the vehicle sideslip based on a nonlinear dynamic model.

The present work follows the line of thought in Klier et al. (2008) but aims at developing a vehicle motion estimation

2405-8963
Peer review under responsibility of International Federation of Automatic Control.
10.1016/j.ifacol.2018.09.091

scheme based on a deterministic observer. Considering the constant improvements of inertial sensors, the proposed approach relies on a kinematic estimator bolstered by a single-track-model-based measurement. The system is represented in a state-affine form, which considerably simplifies the endeavour of designing a deterministic observer. Furthermore, an observability analysis is presented, which theoretically proves the global exponential convergence for the observer design. With the aim of reducing the effect of the single-track model inaccuracies, a tuning rule is suggested that diminishes the impact of the single-track model when its information is superfluous. An online observability evaluation of the system without the model-based measurement equation is performed in order to assess the dispensability of the single-track model. To the authors' best knowledge, a deterministic nonlinear observer design based on the kinematic approach and bolstered by the single-track model is still missing in the literature.

2. MODELLING

The proposed approach is built upon the rigid body kinematic differential equations. The estimation of the vehicle motion states relies on the measurements supplied by a 6-DOF MEMS IMU, i.e., the angular rates (ω_x, ω_y, ω_z) around the body-fixed coordinate system and the accelerations (a_x^s, a_y^s, a_z^s) along the corresponding axes (see Fig. 1). The superscript s indicates that the accelerations are measured and thus contain a component of the gravitational acceleration. The correction of the sensor errors and the perfect alignment between the IMU and body-fixed coordinate system is assumed. The calibration of the IMU is beyond the focus of this paper. In the subsequent discussion, the time dependence has been omitted when not indispensable.

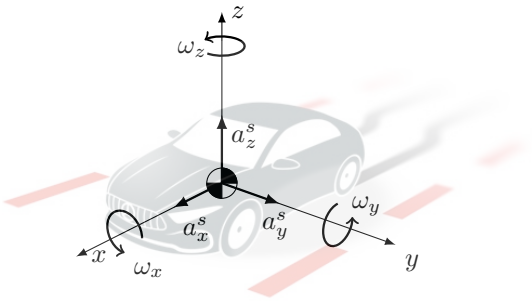

Fig. 1. Body-fixed coordinate system and IMU accelerations and angular rates.

2.1 Vehicle Model

The orientation of the body-fixed coordinate system with respect to the ENU navigation frame (East, North, Up) is described by the intrinsic Euler angles (Ψ, Θ, Φ) with rotations about the axis z, y and x (in that order). Using the IMU angular velocities, the differential equations of the orientation angles read (Wendel, 2011):

$$\begin{aligned}\dot{\Theta} &= \omega_y \cos\Phi - \omega_z \sin\Phi \\ \dot{\Phi} &= \omega_x + \omega_y \sin\Phi \tan\Theta + \omega_z \cos\Phi \tan\Theta \\ \dot{\Psi} &= \omega_y \frac{\sin\Phi}{\cos\Theta} + \omega_z \frac{\cos\Phi}{\cos\Theta}\end{aligned} \tag{1}$$

Since the yaw angle (Ψ) is an isolated variable with no influence on the velocities, its equation is henceforth ignored. After decomposing the gravitation (g) into its respective components in the body-fixed coordinate system, the differential equations of the body-fixed velocity can be expressed as follows (Klier et al., 2008):

$$\begin{pmatrix}\dot{v}_x \\ \dot{v}_y \\ \dot{v}_z\end{pmatrix} = \begin{pmatrix}a_x^s \\ a_y^s \\ a_z^s\end{pmatrix} - \begin{pmatrix}\omega_x \\ \omega_y \\ \omega_z\end{pmatrix} \times \begin{pmatrix}v_x \\ v_y \\ v_z\end{pmatrix} + \begin{pmatrix}g \sin\Theta \\ -g \sin\Phi \cos\Theta \\ -g \cos\Phi \cos\Theta\end{pmatrix} \tag{2}$$

The classic single-track model provides a simplified but plausible description of the vehicle lateral motion within the region of low lateral dynamics, i.e., up to $4\,\mathrm{m/s^2}$ under dry road conditions. In this context the lateral velocity may be expressed as follows (Rodrigo Marco et al., 2018):

$$v_y = l_r\,\omega_z - SG\,a_y^s\,v_x \tag{3}$$

where l_r is the distance of the center of gravity to the rear axle and SG the side slip angle gradient, a constant vehicle parameter.

Even though in most circumstances a vehicle remains within the validity region of the single-track model, during high lateral dynamic manoeuvres (e.g. collision avoidance) or under adverse road conditions (e.g. wet, with snow or ice) its accuracy considerably decreases. Moreover, in the range of high lateral dynamics, where a_y^s takes larger values, the uncertainties in SG have a greater impact. Hence, the use of the single-track model should be restricted.

2.2 State space representation

In order to avoid the use of trigonometric functions and represent the nonlinear system in a state-affine form, the following state vector is defined:

$$\begin{aligned}\boldsymbol{x} &= (\sin\Theta, \sin\Phi\,\cos\Theta, v_x, v_y, v_z, \rho)^T \\ \rho &= \cos\Theta\,\cos\Phi = \sqrt{1-\sin^2\Theta-(\sin\Phi\,\cos\Theta)^2} \\ &= \sqrt{1-x_1^2-x_2^2}\end{aligned} \tag{4}$$

Note that states x_1, x_2 and x_6 correspond to the body fixed coordinates of the ENU z axis ($[0,0,1]$). Using equations (1) and (4) the time derivatives of the first two states can be expressed as follows:

$$\begin{aligned}\dot{x}_1 &= \cos\Theta\,\dot{\Theta} = \omega_y\,\cos\Theta\,\cos\Phi - \omega_z\,\cos\Theta\,\sin\Phi \\ &= \omega_y\,x_6 - \omega_z\,x_2\end{aligned} \tag{5}$$

$$\begin{aligned}\dot{x}_2 &= \cos\Theta\,\cos\Phi\dot{\Phi} - \sin\Theta\,\sin\Phi\,\dot{\Theta} \\ &= \omega_x\,\cos\Theta\,\cos\Phi + \omega_z\,\sin\Theta = \omega_x\,x_6 + \omega_z\,x_1\end{aligned} \tag{6}$$

Combining equations (5)-(6), the time derivative of the sixth state reads:

$$\dot{x}_6 = \frac{-2x_1\,\dot{x}_1 - 2x_2\,\dot{x}_2}{2\,x_6} = -\omega_y\,x_1 - \omega_x\,x_2 \tag{7}$$

It is assumed that the sine of the pitch (Θ) and roll angle (Φ) remain inside the first and fourth quadrant, which occurs in all scenarios but when rolling over. Combining equations (2), (5), (6) and (7), the following state space model is obtained:

$$\begin{aligned}
\dot{x}_1 &= \omega_y\, x_6 - \omega_z\, x_2 \\
\dot{x}_2 &= \omega_x\, x_6 + \omega_z\, x_1 \\
\dot{x}_3 &= \omega_z\, x_4 - \omega_y\, x_5 + g\, x_1 + a_x^s \\
\dot{x}_4 &= -\omega_z\, x_3 + \omega_x\, x_5 - g\, x_2 + a_y^s \\
\dot{x}_5 &= \omega_y\, x_3 - \omega_x\, x_4 - g\, x_6 + a_z^s \\
\dot{x}_6 &= -\omega_y\, x_1 - \omega_x\, x_2
\end{aligned} \tag{8}$$

As for the observation model, the following outputs and measurement equations are employed:

$$\boldsymbol{y} = (v_x, l_r\, \omega_z, v_z)^T = h(\boldsymbol{x}, \boldsymbol{u}) \tag{9}$$

$$\begin{aligned}
h_1 &= x_3 \\
h_2 &= x_4 + SG\, x_3\, a_y^s \\
h_3 &= x_5
\end{aligned} \tag{10}$$

where the second measurement equation is obtained from (3), $\boldsymbol{u} = \left(\omega_x, \omega_y, \omega_z, a_x^s, a_y^s, a_z^s\right)^T$ and the elements in $\boldsymbol{y}$ are measurable quantities.

The system (8)-(10) takes the form of a state-affine system

$$\begin{cases} \dot{\boldsymbol{x}} = A(\boldsymbol{u})\boldsymbol{x} + B(\boldsymbol{u}) \\ \boldsymbol{y} = C(\boldsymbol{u})\boldsymbol{x} \end{cases} \tag{11}$$

where A, B, C are matrices dependent on $\boldsymbol{u}$ obtained from equation (8) and (10).

3. NONLINEAR OBSERVER DESIGN

As the demand for NLOs has increased in several relevant engineering applications, the scientific community has ramped up their own initiative to address this challenge. Due to the massive complexity of developing a general approach applicable to all nonlinear systems, techniques specific for certain types of nonlinear systems have been developed.

In this section an observer design for state-affine systems is presented. It is first proved that any input of the analysed system is *regularly persistent*, an observability condition required for the observer's stability. Due to the limitations of the single-track model, it would be beneficial to use its information when strictly necessary. To this effect, an observer tuning rule depending on the observability properties of the system without the model-based measurement equation is suggested.

3.1 Observer for state-affine systems

The main advantage of designing an observer for a state-affine system is that, under certain conditions on $\boldsymbol{u}$, the dependence on the inputs of the matrices in (11) can be treated as a dependence on time. Therefore, the well-studied theory of linear time-varying systems may be recalled for this class of nonlinear systems. This fact was recognised and exploited by a group of scientists, who presented a solution for the observation problem of state-affine systems.

Bearing in mind the definition of the so-called *observability Gramian* for state-affine systems (Besançon, 2007),

$$W_o(t-T,t) = \int_{t-T}^{t} \Phi_{\boldsymbol{u}}^T(\tau, t-T) C^T(\boldsymbol{u}(\tau)) C(\boldsymbol{u}(\tau)) \Phi_{\boldsymbol{u}}(\tau, t-T) d\tau \tag{12}$$

where $\Phi_{\boldsymbol{u}}(\tau, t)$ is the transition matrix classically defined by

$$\frac{d\Phi_{\boldsymbol{u}}(\tau,t)}{d\tau} = A(u(\tau))\Phi_{\boldsymbol{u}}(\tau,t), \Phi_{\boldsymbol{u}}(t,t) = I \tag{13}$$

with I the identity matrix with the corresponding dimensions. Let us define the concept of *regularly persistent* inputs (Besançon, 2007):

Definition 3.1. *For state-affine systems, an input $\boldsymbol{u}$ is regularly persistent if there exist $T > 0$ and $\alpha > 0$ such that for every $t \geq 0$:*

$$W_o(t-T,t) \geq \alpha I \tag{14}$$

In short, *regularly persistent* inputs steadily allow the unique determination of the states. Bearing this in mind, a solution for the observation of state-affine systems reads (Couenne, 1990):

Theorem 3.1. *Given a state-affine system (11) in which $A(\boldsymbol{u})$, $B(\boldsymbol{u})$, $C(\boldsymbol{u})$ are bounded. For any regularly persistent input, the system*

$$O = \begin{cases} \dot{\hat{\boldsymbol{x}}} &= A(\boldsymbol{u})\hat{\boldsymbol{x}} - R^{-1}C(\boldsymbol{u})^T Q(C(\boldsymbol{u})\hat{\boldsymbol{x}} - \boldsymbol{y}) + B(\boldsymbol{u}) \\ \dot{R} &= -\theta R - A^T(\boldsymbol{u})R - RA(\boldsymbol{u}) + C^T(\boldsymbol{u})QC(\boldsymbol{u}) \\ R(0) &= R_0 \text{ (Symmetric Positive Definite)} \end{cases} \tag{15}$$

with $\theta > 0$ and Q a symmetric positive definite matrix, is an observer of the system (11), whose estimation error decays exponentially with a rate of decay tunable via θ.

Hence, if it can be shown that all inputs of the system defined in (8)-(10) are *regularly persistent*, (15) is a global exponential observer. This can be achieved by analysing the injectivity of the mapping $\Psi_{\boldsymbol{u},N}$ from $\mathbb{R}^n$ into $\mathbb{R}^{Np}$, defined for t, by:

$$\boldsymbol{x} \mapsto \Psi_{\boldsymbol{u},N}(t, \boldsymbol{x}) := \begin{pmatrix} \boldsymbol{y}(t) \\ \dot{\boldsymbol{y}}(t) \\ \vdots \\ \boldsymbol{y}^{(N)}(t) \end{pmatrix} \tag{16}$$

where $N \geq 0$ and p and n are respectively the number of outputs and states in (11). If $\exists N$ such that $\Psi_{\boldsymbol{u},N}$ is injective for all t and $\boldsymbol{u}$, *regular persistence* is guaranteed (Besançon, 2016).

Let's choose $N = 1$, using the Lie Algebra, the output time derivatives can be expressed as a function of the states:

$$\begin{aligned}
y_1 &= L_f^0(h_1) = x_3 \\
y_2 &= L_f^0(h_2) = SGa_y^s x_3 + x_4 \\
y_3 &= L_f^0(h_3) = x_5 \\
\dot{y}_1 &= L_f^1(h_1) = \omega_z x_4 - \omega_y x_5 + g x_1 + a_x^s \\
\dot{y}_2 &= L_f^1(h_2) = -g x_2 + (SG\dot{a}_y^s - \omega_z)x_3 + \omega_x x_5 + \\
&\qquad a_y^s(1 + SG(a_x^s + g x_1 + \omega_z x_4 - \omega_y x_5)) \\
\dot{y}_3 &= L_f^1(h_3) = \omega_y x_3 - \omega_x x_4 - g x_6 + a_z^s
\end{aligned} \tag{17}$$

If the determinant of the Jacobian $\frac{\partial \Psi_{\boldsymbol{u},1}}{\partial \boldsymbol{x}}$ is nonzero independently of $\boldsymbol{u}$ and $\boldsymbol{x}$, then the injectivity is proved. Taking partial derivatives, the Jacobian is obtained:

$$\frac{\partial \Psi_{\boldsymbol{u},1}}{\partial \boldsymbol{x}} = \begin{pmatrix} 0 & 0 & 1 & 0 & 0 & 0 \\ 0 & 0 & a_0 & 1 & 0 & 0 \\ 0 & 0 & 0 & 0 & 1 & 0 \\ g & 0 & 0 & \omega_z & -\omega_y & 0 \\ g\,a_0 & -g & \dot{a}_0 - \omega_z & a_0\,\omega_z & \omega_x - a_0\,\omega_y & 0 \\ 0 & 0 & \omega_y & -\omega_x & 0 & -g \end{pmatrix}$$
$$a_0 = SG\,a_y^s \tag{18}$$

Its determinant is $g^3 \neq 0$. Thus, all inputs $\boldsymbol{u}$ of the system defined in (8)-(10) are *regularly persistent* and (15) is a global exponential observer for the system.

3.2 Observability-based tuning

As already seen in Section 2, the second measurement equation of the system is based on the single-track model, see equation (10). The accuracy of the information that it provides is restricted to its validity region and depends on the correctness of the parameter SG. Hence, it seems coherent to ask oneself whether it is possible to estimate all the states without this information. Let us define

$$\boldsymbol{y_{red}} = \begin{pmatrix} v_x \\ v_z \end{pmatrix} = h_{\mathrm{red}}(\boldsymbol{x}, \boldsymbol{u}) = C_{\mathrm{red}}\,\boldsymbol{x} = \begin{pmatrix} x_3 \\ x_5 \end{pmatrix} \tag{19}$$

as the measurement model without the single-track model information (*reduced measurement model*).

It has been observed that under poor lateral excitation, the system with the *reduced measurement model* loses observability (Klier et al., 2008). This can also be shown analytically. When considering the case where the vehicle is driving in a straight line at a constant velocity, the angular rate as well as the acceleration and velocity time derivatives become negligible. In this case, the outputs and their time derivatives take the following form:

$$\begin{aligned} y_1 &= v_x = x_3 \\ y_3 &= v_z = x_5 \\ \dot{y}_1 &= 0 = g\,x_1 + a_x^s \\ \dot{y}_3 &= 0 = -g\,x_6 + a_z^s \\ \ddot{y}_1 = \ddot{y}_3 &= \ldots = y_1^{(N)} = y_3^{(N)} = 0 \end{aligned} \tag{20}$$

Clearly, the problem described in (20) is underdetermined. Therefore, under these inputs, the injectivity of $\Psi_{\boldsymbol{u},N}$ is not guaranteed, i. e., the system states cannot be uniquely determined from the knowledge of the available information (inputs, outputs and their time derivatives). This implies that not all possible inputs are *regularly persistent*. Therefore, if the single-track model is completely neglected, under some inputs, the observer will not converge (similar results are obtained when standing still).

An approach to overcome the described difficulties is to increase the importance of the single-track model information when necessary and reduce it when superfluous. If the excitation is too low to guarantee the *regularly persistent* property for the system with the *reduced measurement model*, the single-track model information is necessary and therefore highly weighted. Otherwise, it is superfluous and its weight is set lower. This can be done by tuning the elements of Q, which works to some extent as a gain for the measurement error, see (15). In doing so, the single-track model is effectively used when strictly necessary.

In order to identify when the single-track model information is superfluous, one needs to test the *regularly persistent* property for the system with the *reduced measurement model*. Since the complexity of the injectivity analysis of $\Psi_{\boldsymbol{u},N}(t, \boldsymbol{x})$ escalates in this case, other approaches must be investigated. In this context, the *observability Gramian* may be analysed. Computing the *observability Gramian* from (12) is a cumbersome task since the transition matrix is required. Fortunately, there is a more feasible approach, which consists in the backwards integration of the *observability Gramian*'s time derivative (Crassidis and Junkins, 2011). In our case, where $C(u(t)) = C_{\mathrm{red}}$, the time derivative reads:

$$\begin{aligned} &\dot{W}_{o,\mathrm{red}}(\tau, t) = \\ &-A^T(u(\tau))W_{o,\mathrm{red}}(\tau, t) - W_{o,\mathrm{red}}(\tau, t)A(u(\tau)) - C_{\mathrm{red}}^T C_{\mathrm{red}} \end{aligned} \tag{21}$$

with $W_{o,\mathrm{red}}(t, t) = 0$.

As seen in *Definition 3.1*, the singularity of $W_{o,\mathrm{red}}(t-T, t)$ is directly connected to the *regularly persistent* property. If $W_{o,\mathrm{red}}(t-T, t)$ is singular, the inputs are not *regularly persistent*, i. e., the information obtained with the *reduced measurement model* is insufficient for a state reconstitution in the time interval $[t-T, t]$. In this case, the single-track model information is necessary.

In order to assess the *regular persistence* online, one could track the value of the determinant of $W_{o,\mathrm{red}}(t-T, t)$, hereafter also referred as the chosen *observability index*. Limits can be set so that over a particular threshold (h_{det}) the single-track model information is certainly dispensable and below other (l_{det}) this information is necessary. Therefore, in the former case, the corresponding element in Q is chosen low ($q_{22,\mathrm{obs}}$). In the latter case, a larger value is assigned ($q_{22,\overline{\mathrm{obs}}}$). In between a fuzzy area is found. For this interval a fading function can be implemented, which additionally smooths the transition:

$$q_{22} = \mathrm{fade}(|\det(W_{o,\mathrm{red}}(t-T, t))|, l_{\mathrm{det}}, h_{\mathrm{det}}, q_{22,\overline{\mathrm{obs}}}, q_{22,\mathrm{obs}}) \tag{22}$$

where "fade" represents a continuous fading function such as exponential or arctangent. Note that the proof of *Theorem 3.1* is valid for a Q that adapts as described. The presented estimation scheme (Alg. 1) is based on a global exponential observer. Furthermore it reduces the single-track model influence on the estimates whenever this information is superfluous. Thereby, the impact of model inaccuracies during periods of high lateral excitation may be avoided.

Algorithm 1: Estimation scheme with observability-based tuning

$k = k + 1$;
Observability adaptation
$W_{o,\mathrm{red},k} = \int_{t_k}^{t_k - T} \dot{W}_{o,\mathrm{red}}(\tau, t_k)d\tau, W_{o,\mathrm{red}}(t_k, t_k) = 0$;
$q_{22,k} = \mathrm{fade}(|\det(W_{o,\mathrm{red},k})|, l_{\mathrm{det}}, h_{\mathrm{det}}, q_{22,\overline{\mathrm{obs}}}, q_{22,\mathrm{obs}})$
$Q_k = \mathrm{diag}(q_{11}, q_{22,k}, q_{33})$;
Observer integration
$[\hat{\boldsymbol{x}}_k, R_k] = \mathrm{ODESolverUpdate}(O(\hat{\boldsymbol{x}}_{k-1}, R_{k-1}, \boldsymbol{u}_k, \boldsymbol{y}_k, Q_k))$;
Notes
$W_{o,\mathrm{red},k} = W_{o,\mathrm{red}}(t_k - T, t_k)$.
ODESolverUpdate corresponds to the update function of an ODE numerical solver (e.g. Euler, Adams-Bashforth...) based on the observer's differential equations (O) defined in (15).

4. EXPERIMENTAL RESULTS

The effectiveness of the proposed estimation scheme is exemplified with experimental tests conducted on a car with rear wheel drive. The test vehicle is equipped with a high-precision IMU/GNSS deeply coupled inertial navigation system. This relies on an RTK (Real Time Kinematic) GNSS and a high-performance inertial measurement system, which consists of fiber optic gyroscopes and MEMS-based servo accelerometers. The system inputs, i.e., angular rates (ω_x, ω_y, ω_z) and accelerations (a_x^s, a_y^s, a_z^s) are obtained from its IMU. Ground truth velocities and attitude angles can be obtained by processing the signals it supplies. The measurements v_x and v_z are directly taken from the ground truth velocities. Notice that the aim of this section is to evaluate the performance of the estimation scheme presented in Alg. 1 and not the accuracy of the measured velocities. Calculating reference longitudinal and vertical velocities is out of the scope of the present work. Nevertheless, this has been intensively studied in the context of Electronic Stability Control, see e.g. Gao et al. (2013); Klier et al. (2008). Both inputs and measurements are supplied to the system at a sampling rate of 100Hz, which is also the estimator's update frequency.

In order to demonstrate the effectiveness of the presented approach, three estimation schemes are compared:

(A) Observer O from (15) based on the system with the *reduced measurement model* (19)
(B) Observer O from (15) based on the system with the original measurement model (9)-(10)
(C) Estimation scheme presented in Alg. 1

Table 1: Estimator scheme parameter choice, units according to the International System of Units.

Parameter	Value	Comment
θ	0.8	see (15)
$R(0)$,(R_0)	$0.1I_6$	see (15)
T	0.45	see (12) and Alg. 1
$q_{22,\overline{\text{obs}}}$	1	see Alg. 1
$q_{22,\text{obs}}$	10^{-5}	see Alg. 1
q_{11}	10	see Alg. 1
q_{33}	10	see Alg. 1
$\hat{\boldsymbol{x}}(0)$,$(\hat{\boldsymbol{x}}_0)$	$\left(0,0,0,0,0,1\right)^T$	see (15)
l_{det}	$0.5 \cdot 10^{-13}$	see Alg. 1
h_{det}	$2 \cdot 10^{-13}$	see Alg. 1

It is well-known that the choice of the tuning parameters significantly influences the performance of observers. The observer parametrization as well as the l_{det} and h_{det} choice (see Table 1) are built upon experimental results obtained from different manoeuvres such as circle, slalom and figure eight drives. In the subsequent analysis the observer's parameters are the same for all approaches. The only exception is Q, for scheme (A) $Q = (q_{11}, q_{33})^T$, for (B) $Q = \left(q_{11}, q_{22,\overline{\text{obs}}}, q_{33}\right)^T$ and for (C) as defined in Alg. 1.

The presented estimation scheme has been run on measurement data from a drive on a test track. It contains interesting motions for our application such as standstill phases, straight-ahead driving, regular turns and dynamic turns. Fig. 2 and Fig. 3 show the velocity and attitude estimation errors respectively. Fig. 4 presents a deeper insight in the lateral motion profile of the manoeuvre.

In Subsection 3.2 it has been analytically proved that for the system with the *reduced measurement model* the *regular persistence* property is lost while standing still or driving straight. This is also confirmed by the chosen *observabiltiy index*, see Fig. 4 (e.g. $t = [0, 20]$ s and $t = [155, 170]$ s). On the other hand, under lateral excitation, the *observability index* substantially increases (e.g. $t = [210, 300]$ s). This behaviour is reflected in the velocity and attitude estimates from (A), see Fig. 2 and Fig. 3. The estimates present large deviations from the ground truth during straight-ahead driving and standstill phases and converge whenever there is lateral excitation.

Scheme (B) presents a more robust behaviour. Nonetheless, its estimated errors considerably increase in those turns where the validity limits of the single-track model are transcended, i. e., when $a_y > 4\,\text{m/s}^2$ (e.g. $t = [210, 300]$ s). In less dynamic turns the errors are similar to those of scheme (A) (e.g. $t = [70, 75]$ s). Note that deviation is more evident for v_y and ϕ. This is logical since these are the states directly affected by the lateral motion and hence by the single-track model. Furthermore, v_x and v_z are directly measured states.

The benefits of approaches (A) and (B) are combined in the estimation scheme (C), whose estimates present a significantly improved behaviour. In this case, the information of the single-track model is effectively used when strictly necessary, i.e. in periods of poor lateral excitation. This corresponds to its validity region and where the uncertainty in SG has low influence. During dynamic turns, where the model limitations are surpassed, this information is superfluous and hence its influence is reduced. As illustrated in Fig.2 and Fig.3, the result is an estimation scheme without observability issues, which additionally is robust against the single-track model inaccuracies.

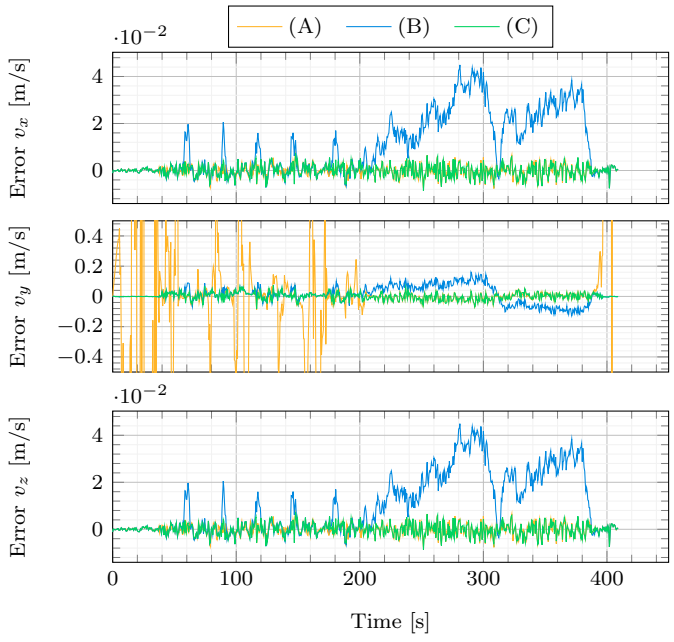

Fig. 2. Velocity estimate errors for the three approaches. $\hat{x}_3 - v_{x,GT}$ (top), $\hat{x}_4 - v_{y,GT}$ (middle), $\hat{x}_5 - v_{z,GT}$ (bottom). The ground truth (GT) velocities are obtained from the ENU velocities supplied by the high-precision navigation system.

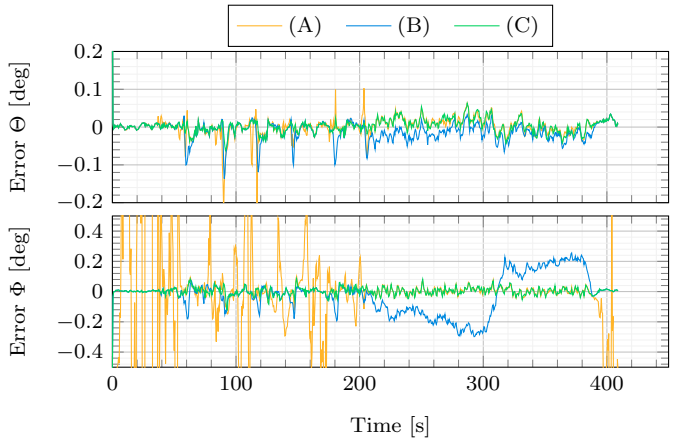

Fig. 3. Attitude angle estimate errors for the three approaches. $\hat{\Theta} - \Theta_{GT}$ (top), $\hat{\Phi} - \Phi_{GT}$ (bottom). The ground truth (GT) attitude angles are directly obtained from the high-precision navigation system.

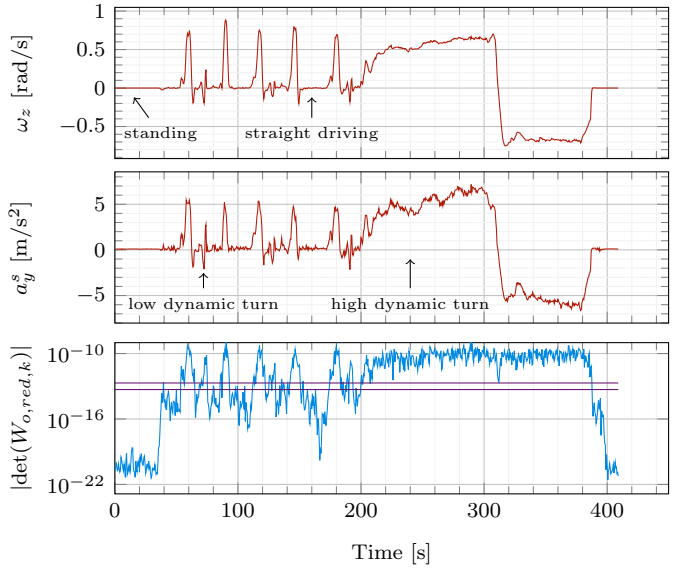

Fig. 4. Lateral dynamics and observability assessment results. The yaw rate ω_z (top, red), lateral acceleration a_y^s (middle, red) and $|\det(W_{o,red,k})|$ (bottom, blue) together with the thresholds $l_{\det}$ and $h_{\det}$ (violet).

5. CONCLUSION

This paper demonstrates how existing NLOs techniques can be effectively adapted to tackle a vehicle motion estimation problem. The presented scheme relies on the combination of the kinematic model-based approach with a dynamic model-based measurement equation. The global exponential convergence for the NLO design is theoretically proved by means of an in-depth observability analysis. For the purpose of reducing the effect of the dynamic model inaccuracies, an observability-based tuning rule is presented. The adaptation diminishes the single-track model's impact on the estimates when the information of the single-track model becomes superfluous. The effectiveness of the method has been demonstrated on actual data collected from a test vehicle. The presented approach has shown good stability properties and robustness against the dynamic model inaccuracies.

REFERENCES

Antonov, S., Fehn, A., and Kugi, A. (2011). Unscented kalman filter for vehicle state estimation. *Vehicle System Dynamics*, 49(9), 1497–1520.

Besançon, G. (2016). A link between output time derivatives and persistent excitation for nonlinear observers. 49(18), 493 – 498. 10th IFAC Symposium on Nonlinear Control Systems NOLCOS 2016.

Besançon, G. (2007). *An Overview on Observer Tools for Nonlinear Systems*, 1–33. Springer Berlin Heidelberg, Berlin, Heidelberg.

Brunker, A., Wohlgemuth, T., Frey, M., and Gauterin, F. (2017). Gnss-shortages-resistant and self-adaptive rear axle kinematic parameter estimator (sa-rakpe). In *2017 IEEE Intelligent Vehicles Symposium (IV)*, 456–461.

Bryne, T.H., Hansen, J.M., Rogne, R.H., Sokolova, N., Fossen, T.I., and Johansen, T.A. (2017). Nonlinear observers for integrated ins/gnss navigation: Implementation aspects. *IEEE Control Systems*, 37(3), 59–86.

Couenne, N. (1990). *Synthèse d'Observateurs de Systèmes Affines en l'État*. Theses, Institut National Polytechnique de Grenoble - INPG.

Crassidis, J.L. and Junkins, J.L. (2011). *Optimal estimation of dynamic systems*. CRC press.

Gao, Y., Feng, Y., and Xiong, L. (2013). *Vehicle Longitudinal Velocity Estimation with Adaptive Kalman Filter*, 415–423. Springer Berlin Heidelberg, Berlin, Heidelberg.

Grip, H.F., Imsland, L., Johansen, T.A., Kalkkuhl, J.C., and Suissa, A. (2009). Vehicle sideslip estimation. *IEEE Control Systems*, 29(5), 36–52.

Hrgetic, M., Deur, J., Ivanovic, V., and Tseng, E. (2014). Vehicle sideslip angle ekf estimator based on nonlinear vehicle dynamics model and stochastic tire forces modeling. *SAE International Journal of Passenger Cars - Mechanical Systems*, 7(1), 86–95.

Katriniok, A. and Abel, D. (2016). Adaptive ekf-based vehicle state estimation with online assessment of local observability. *IEEE Transactions on Control Systems Technology*, 24(4), 1368–1381.

Klier, W., Reim, A., and Stapel, D. (2008). Robust estimation of vehicle sideslip angle - an approach w/o vehicle and tire models. In *SAE Technical Paper*. SAE International.

Piyabongkarn, D., Rajamani, R., Grogg, J.A., and Lew, J.Y. (2009). Development and experimental evaluation of a slip angle estimator for vehicle stability control. *IEEE Transactions on Control Systems Technology*, 17(1), 78–88.

Rodrigo Marco, V., Kalkkuhl, J., and Raisch, J. (2018). Ekf for simultaneous vehicle motion estimation and imu bias calibration with observability-based adaptation. In *2018 American Control Conference (ACC)*.

Song, Y. and Grizzle, J.W. (1992). The extended kalman filter as a local asymptotic observer for nonlinear discrete-time systems. In *American Control Conference, 1992*, 3365–3369. IEEE.

Wendel, J. (2011). *Integrierte Navigationssysteme: Sensordatenfusion, GPS und Inertiale Navigation*. Walter de Gruyter.

Weydert, M. (2012). Model-based ego-motion and vehicle parameter estimation using visual odometry. In *2012 16th IEEE Mediterranean Electrotechnical Conference*, 914–919.